Role of spin-lattice coupling in ultrafast demagnetization and all optical helicity-independent single-shot switching in Gd1−x−yTbyCox alloys

Wei Zhang, Jun Xiao Lin, Tian Xun Huang, Grégory Malinowski, Michel Hehn, Yong Xu, Stéphane Mangin, Weisheng Zhao

Role of spin-lattice coupling in ultrafast demagnetization and all optical helicity-independent single-shot switching in $Gd_{1-x-y}Tb_yCo_x$ alloys

Wei Zhang,[1,2,3] Jun Xiao Lin,[3] Tian Xun Huang,[3] Gregory Malinowski,[3] Michel Hehn,[3] Yong Xu,[1,2,*] Stéphane Mangin,[3,†] and Weisheng Zhao[1,2]

[1]*Anhui High Reliability Chips Engineering Laboratory, Hefei Innovation Research Institute, Beihang University, Hefei 230013, China*
[2]*MIIT Key Laboratory of Spintronics, School of Integrated Circuit Science and Engineering, Beihang University, Beijing 100191, China*
[3]*Université de Lorraine, CNRS, IJL, F-54000 Nancy, France*

(Received 17 October 2021; revised 13 January 2022; accepted 31 January 2022; published 11 February 2022)

All optical switching (AOS) of magnetization exhibits a high potential for ultrafast and energy-efficient memory applications. Many works have been carried out in the area of AOS, including its observation in a wide variety of ferromagnetic or ferrimagnetic materials, and the exploration of the parameters for the achievements of AOS such as the laser fluence and helicity, and duration of laser pulses. A large majority of all optical helicity-independent single-shot switching (AO-HIS) has been observed in Gd-based rare-earth transition-metal ferrimagnets. It is then necessary to explore the unique role of Gd in AO-HIS mechanism, compared with other rare-earth elements. Here, we engineered $Gd_{1-x-y}Tb_yCo_x$ alloys and investigated the influence of the Tb concentration on the magnetization dynamics via static Kerr microscope and time-resolved magneto-optical Kerr effect (TR-MOKE) measurements. The ultrafast demagnetization time at low fluence is found to be independent of Tb concentration, while both the range of laser fluence and pulse duration allowing for AO-HIS becomes narrower with increasing the Tb concentration. The TR-MOKE signal $\Delta\Theta_K/\Theta_{K\_sat} \sim 10$ ps after the laser pulse excitation decreases with increasing either the Tb concentration or the pulse duration. The fact that AO-HIS is prohibited by increasing the Tb content is explained by considering a larger damping for Tb than Gd in atomistic simulations. Our results are well explained by the fact that angular momentum can be transferred from Gd to Co resulting in the magnetization switching, whereas for Tb it is dissipated through the lattice due to the large spin-orbit coupling, instead of being transferred between Tb and Co.

DOI: 10.1103/PhysRevB.105.054410

I. INTRODUCTION

Ultrashort laser pulse has the capacity to control magnetization at subpicosecond timescale [1,2]. It is two to three orders of magnitude faster compared to the conventional methods for manipulating spins, including magnetic [3] or electric fields [4], heat [5], strains [6], spin-transfer torque [7], as well as spin-orbit torque [8]. Thus, the interaction between a femtosecond laser pulse and spins in a magnetic system has become a rapidly growing area of science during the past decades. In 2007, Stanciu *et al.* [9] demonstrated all optical switching using circular femtosecond laser pulse in GdFeCo ferrimagnetic rare-earth transition-metal (RE-TM) alloy. Soon after, the major breakthrough was made that a single linearly polarized pulse is sufficient to switch the GdFeCo in picosecond timescale, which is called all optical helicity-independent switching (AO-HIS) [10]. Since these pioneering works, the possibility of manipulating spins with an ultrashort optical laser pulse has great potential for designing technological devices with high-speed, energy-efficient, and nonvolatile magnetic memory storage [11].

Up to now, Gd-based RE-TM alloys or multilayers such as GdFeCo [12,13], GdCo [14], Gd/Co [15], and Co/Pt/Co/GdFeCo [16] systems show deterministic ultrafast toggle switching of the magnetization using a single laser pulse. A large amount of work has been devoted to understand the mechanism of AO-HIS within Gd-based RE-TM alloys. For example, Radu *et al.* reported the presence of two different relaxation times from Gd and FeCo sublattices by time-resolved x-ray magnetic circular dichroism measurements [10]. Apart from the intrinsic magnetic properties of materials, the parameter of laser pulse such as fluence and pulse duration have also been explored [17]. Gorchon *et al.* [18] reported that magnetic switching could even be obtained for a 15-ps-long pulse duration. Furthermore, Davies *et al.* [12] showed that the maximum pulse duration allowing for AO-HIS in GdFeCo depends on the concentration of Gd. Subsequently, Wei *et al.* [19] obtained the AO-HIS state diagrams for GdFeCo thin films for different compositions and thicknesses by determining the magnetic configuration as a function of laser-pulse duration and fluence.

Contrary to the tremendous amount of work reported on Gd-based ferrimagnetic materials, the AO-HIS was very recently demonstrated in synthetic ferrimagnet composed of two distinct transition metal ferromagnetic layers Ni_3Pt and Co [20], Mn_2RuGa [21], and Tb/Co multilayers [22]. In addition, Alebrand *et al.* reported a transient reverse of magnetization in $Tb_{32}Co_{68}$ alloy on a subpicosecond timescale [23]. However, no magnetization reversal was observed on the long timescale in this case. Interestingly, Tb-based RE-TM systems are

*yongxu@buaa.edu.cn
†stephane.mangin@univ-lorraine.fr

capable to support the domains down to nanometer scales due to the much higher spin-orbit coupling in Tb than that in Gd [24], suggesting a promising new kind of material for AO-HIS spintronic devices. However, switching was observed only for a narrow range of concentrations and laser fluences in Tb/Co multilayers [25]. Despite Tb_xCo_{1-x} alloy being argued to satisfy the necessary conditions for AO-HIS on the basis of atomistic simulations [26], it is not yet clearly understood why these Tb-based ferrimagnetic multilayers show AO-HIS experimentally and not the alloys. Moreover, to understand why the Gd-based ferrimagnets easily exhibit AO-HIS as compared to Tb-based alloys, and consequently to expand the materials showing AO-HIS, it is highly desirable to investigate the influence of laser parameters and the magnetic properties of (GdTb) alloy-based ferrimagnetics. Interestingly, Eschenlohr *et al.* [27] investigated the effect of spin-lattice coupling on ultrafast demagnetization by employing the alloy of $Gd_{1-x}Tb_x$. They found that the second demagnetization step occurs faster when increasing the Tb content. This result indicates that the second step of demagnetization taking place at tens of picoseconds is dominated by the spin-lattice coupling of $4f$ electrons and its acceleration with more Tb is due to the stronger spin-lattice coupling in $Gd_{1-x}Tb_x$ as compared to the pure Gd metal. Recently, Andres *et al.* proposed the weaker $4f$ spins and lattice coupling in Gd as compared with Tb is one potential reason to explain why the AO-HIS is usually observed in GdFe, rather than TbFe-based compounds [28]. Ceballos *et al.* reported the role of element-specific damping on all optical switching in $Gd_{22-x}Tb_xCo_{78}$ [29]. The Gilbert damping of Gd was tuned in atomistic simulations [30] to reproduce the magnetization switching dynamics obtained in time-resolved magneto-optical Kerr effect (TR-MOKE). They argued that the lower damping in Gd is responsible for the faster dynamics and lower critical fluences of the Gd dominant alloys. However, the AO-HIS state diagrams as a function of laser-pulse duration and fluence for $Gd_{1-x-y}Tb_yCo_x$ thin films with various x and y are still not clear.

In this paper, we mainly focus on the single-shot all optical switching phenomenon by tuning the Gd, Tb concentration in $Gd_{1-x-y}Tb_yCo_x$ alloys. The spin dynamics taking place from femtosecond to picosecond timescales was studied carefully by means of TR-MOKE. At femtosecond timescale, to study the influence of Tb on ultrafast demagnetization, the ultrafast demagnetization time τ_M is extracted as a function of Tb concentration keeping a constant maximum demagnetization. For AO-HIS at longer timescale, the laser fluence dependence of the $\Delta\Theta_K/\Theta_{K\_sat}$ signal measured at 10 ps after excitation of laser pulse are compared and the AO-HIS state diagrams for GdTbCo thin films as a function of laser-pulse duration and fluence are reported for various composition of Tb and Co. From these measurements, we found a slower remagnetization dynamics, a narrower range of laser fluences for switching, and a reduction of the maximum pulse duration (τ_{max}) for the occurrence of switching with increasing Tb concentration, when the composition of Co is fixed. The above experimental results are attributed to the variation of spin-lattice coupling after alloying Gd and Tb in $Gd_{1-x-y}Tb_yCo_x$ thin films. To understand it quantitatively, the atomistic spin dynamics model was carried out, in which an element-specific damping is assigned to Tb and Gd, respectively, to represent the different spin-lattice coupling. A good agreement between the simulations and the experimental results ranging from femtosecond to picosecond timescales is found.

II. EXPERIMENT RESULTS

A. Sample structure and characterization

We prepared a series of 5-nm-thick $Gd_{1-x-y}Tb_yCo_x$ thin films with $x = 78, 80$, and 84%, while y ranges from 6.1 to 14%, 5.5 to 12.5%, and 4.5 to 11.4%, respectively. The samples are deposited by dc magnetron sputtering onto a glass substrate according to the following multilayered structure: Glass/Ta(3 nm)/Pt(5 nm)/$Gd_{1-x-y}Tb_yCo_x$(5 nm)/Cu(3 nm)/Ta(5 nm). The Ta layer on top prevents the oxidation of the magnetic films, and the bottom Ta layer improves adhesion of the structure on the glass substrate. Based on the magnetic hysteresis loops obtained by static MOKE measurements, all studied samples show strong perpendicular magnetic anisotropy, and all the samples are Co dominant at room temperature (MOKE results are shown in Note 1 within the Supplemental Material) [31].

B. All optical helicity-independent switching of $Gd_{1-x-y}Tb_yCo_x$

AO-HIS was studied by means of both static Kerr microscope and TR-MOKE. In both techniques, a Ti:sapphire fs-laser source with a regenerative amplifier was used to generate the linearly polarized pump laser beam with a central wavelength of 800 nm (1.55 eV). The repetition rate of the fs laser was 5 kHz. Moke microscopy was performed using a light-emitting diode source with a wavelength of 628 nm. In order to perform TR-MOKE measurements, the pump wavelength was kept at 800 nm while the probe was frequency doubled to 400 nm. A biased field larger than the coercivity of each sample was applied during the TR-MOKE measurements while no field was applied in the case of static Kerr microscope measurements. The laser-pulse duration is controlled by appropriate adjustment of a grating-pair compressor.

As shown in Fig. 1, we recorded a group of magneto-optical images for $Gd_{15.9}Tb_{6.1}Co_{78}$ after exposure to laser pulses with different fluences and pulse durations. When $\tau_{pulse} = 50$ fs, the switching takes place for the laser fluence ranging from $F_{switch} = 1.22\ mJ/cm^2$ defining the lowest fluence at a given pulse duration required to observe switching up to $F_{demag} = 3.7\ mJ/cm^2$ above which only multidomain state occurs. Here, the multidomain state occurs when $F = 3.7\ mJ/cm^2$, which is defined as F_{demag}. As τ_{pulse} increases, the range of laser fluence allowing for magnetization switching before reaching a multidomain state becomes narrower up to a certain pulse duration $\tau_{pulse} = 3100$ fs, above which single-shot magnetization switching cannot be achieved anymore and only multidomain patterns can be observed above $F_{demag} = 3.51\ mJ/cm^2$. We determined F_{switch} and F_{demag} for different pulse durations allowing us to produce the state diagrams presented in Fig. 2. Firstly, a general feature independent of the concentration of Tb is observed, that is F_{switch} keeps increasing as the pulse duration τ_{pulse} increases until $F_{switch} = F_{demag}$, which defines the maximum pulse duration (τ_{max}) for which AO-HIS can be observed. Meanwhile, F_{demag}

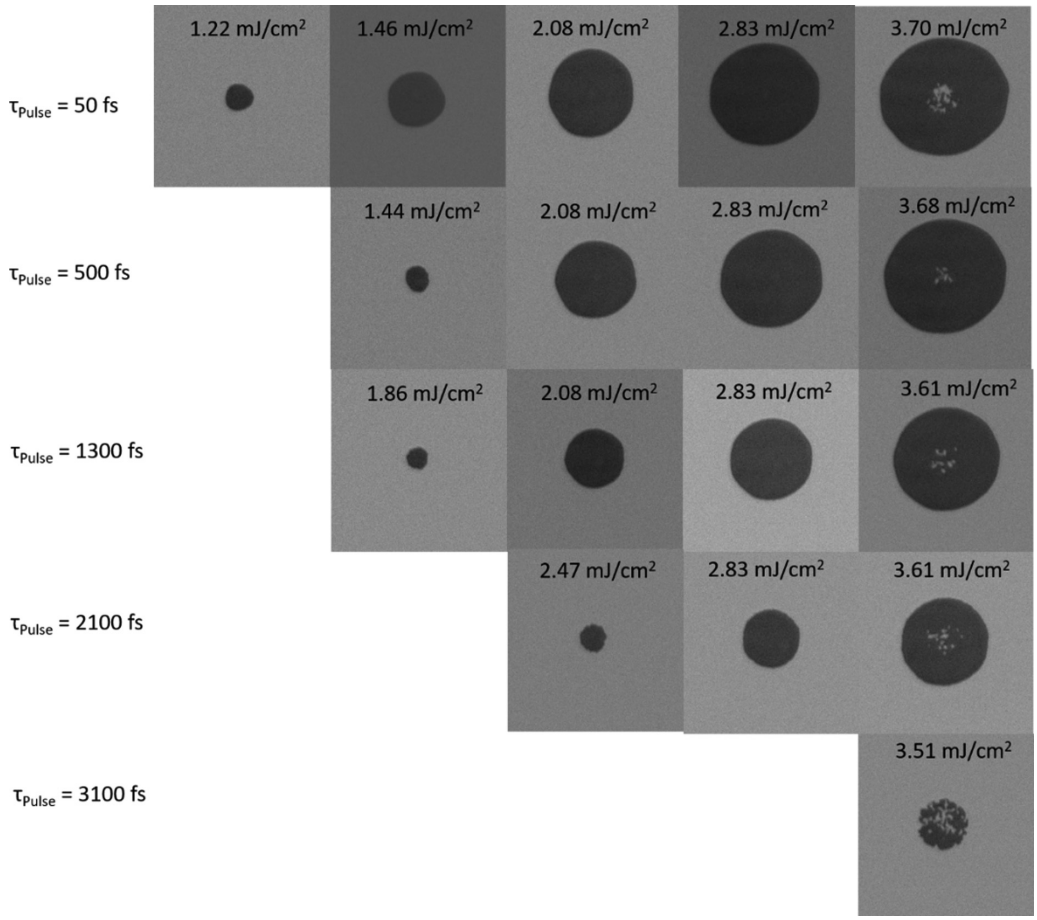

FIG. 1. Magneto-optical images of $Gd_{15.9}Tb_{6.1}Co_{78}$ after exposure to a single linearly polarized laser pulse with a pulse duration of 50, 500, 1300, 2100, and 3100 fs, and with various fluences ranging from 1.22 to 3.7 mJ/cm^2.

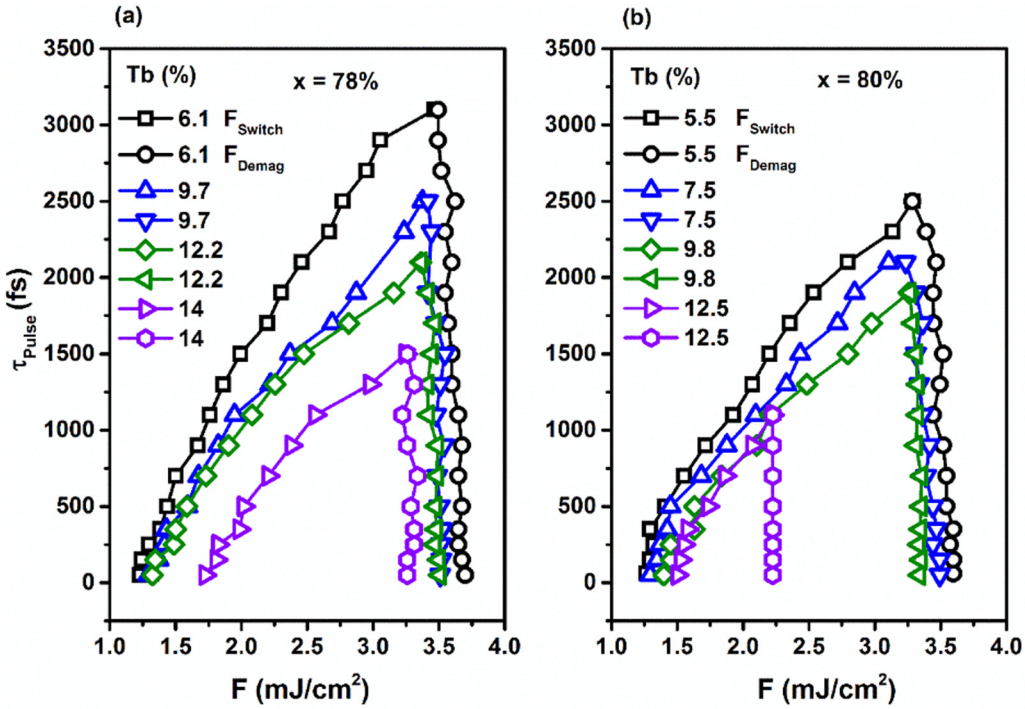

FIG. 2. AO-HIS state diagram for $Gd_{1-x-y}Tb_yCo_x$ thin films with $x = 78, 80\%$, while y ranges from 6.1 to 14% and 5.5 to 12.5%, respectively: switching fluence F_{switch} and demagnetization fluence F_{demag} as a function of the pulse duration for a single linearly polarized laser pulse.

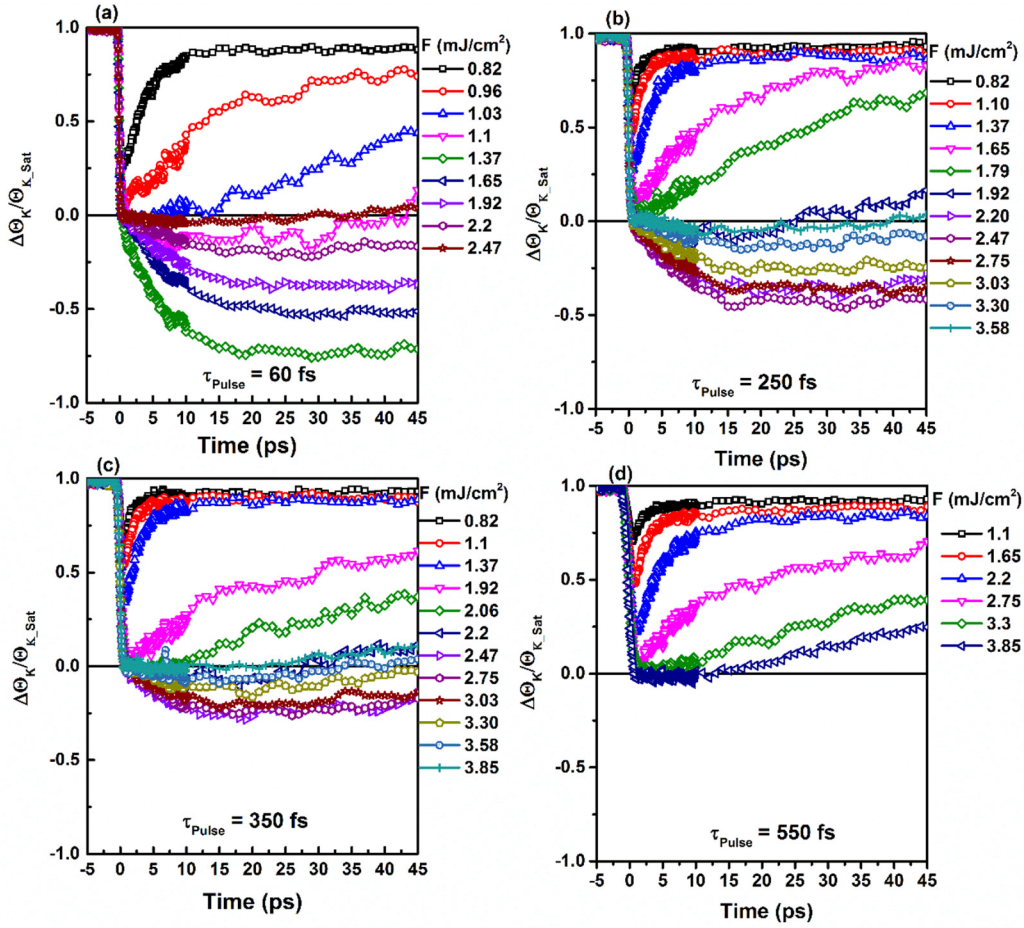

FIG. 3. Laser fluence F-dependent magnetization dynamics of $Gd_{15.9}Tb_{6.1}Co_{78}$ with various laser pulse duration τ_{pulse} ranging from 60 to 550 fs. (a)–(d) Magnetization dynamics as a function of laser fluence for $\tau_{pulse} = 60,\ 250, 350$, and 550 fs.

shows a weak dependence on τ_{pulse}. Secondly, the exact value of both F_{switch} and F_{demag} as well as τ_{max} strongly depends on the concentration of Tb. Indeed, F_{switch} increases, while F_{demag} decreases for higher Tb concentration for a fixed pulse duration. We also found that the fluence range showing AO-HIS is larger and τ_{max} is longer for lower Tb concentrations. For example, τ_{max} decreases from 3100 to 1400 fs with increasing the Tb concentration from 6.1 to 14% when $x = 78\%$. A similar trend is observed for $x = 80\%$. According to Ceballos *et al.* [29], the critical fluence for switching becomes higher as the Tb content increases. It agrees well with our observations. But, in this study, we also focused on the influence of Tb content on the state diagram, including the maximum pulse duration allowing for switching as well as F_{demag}.

The magnetization dynamics as a function of laser fluence in $Gd_{15.9}Tb_{6.1}Co_{78}$ is displayed in Fig. 3 for various laser-pulse durations τ_{pulse}. For $\tau_{pulse} = 60$ fs, when the laser fluence $F < 1.03\ mJ/cm^2$, a rapid magnetization recovery back to the initial state takes place after ultrafast partial demagnetization. With F increasing, the recovery of magnetization becomes slower and the magnetization stays around zero without recovery for several picoseconds when $F = 1.03\ mJ/cm^2$. For fluences larger than $F = 1.03\ mJ/cm^2$, defined as F_{switch}, magnetization switching is observed. For fluences at $F = 2.47\ mJ/cm^2$, a long-lived fully demagnetized state is characterized. So, AO-HIS is only observed for a fluence value between a certain range . When increasing the laser-pulse duration τ_{pulse}, a similar trend is observed as a function of the laser fluence. But, the magnetization switching is forbidden when $\tau_{pulse} = 550$ fs, where the magnetization reaches zero after the laser pulse with $F = 3.85\ mJ/cm^2$ and goes back to the initial state slowly rather than cross zero to reverse. The sample was damaged for fluence larger than $3.85\ mJ/cm^2$. So, in TR-MOKE measurements, F_{demag} was defined as the laser fluence, at which the laser will almost damage the sample. The same measurements were repeated for all the other samples $Gd_{1-x-y}Tb_yCo_x$ with $x = 80, 84\%$ (see Fig. S2, Supplemental Material) [31]. We found that the switching occurs for $x = 78$ and 80%, when the concentration of Tb y is less than 12.2 and 9.8%, respectively. For $x = 84\%$, the switching is prohibited whatever the Tb concentration y is, even at the shortest pulse duration. This is probably due to the fact that the composition of Co 84% is too far away from the compensation point at room temperature as stated within Note 1 of the Supplemental Material [31]. To confirm the switching behavior of magnetization dynamics, magnetization toggle switching demonstrated using static Kerr microscope is shown in Fig. S3 in the Supplemental Material [31]. In addition, the

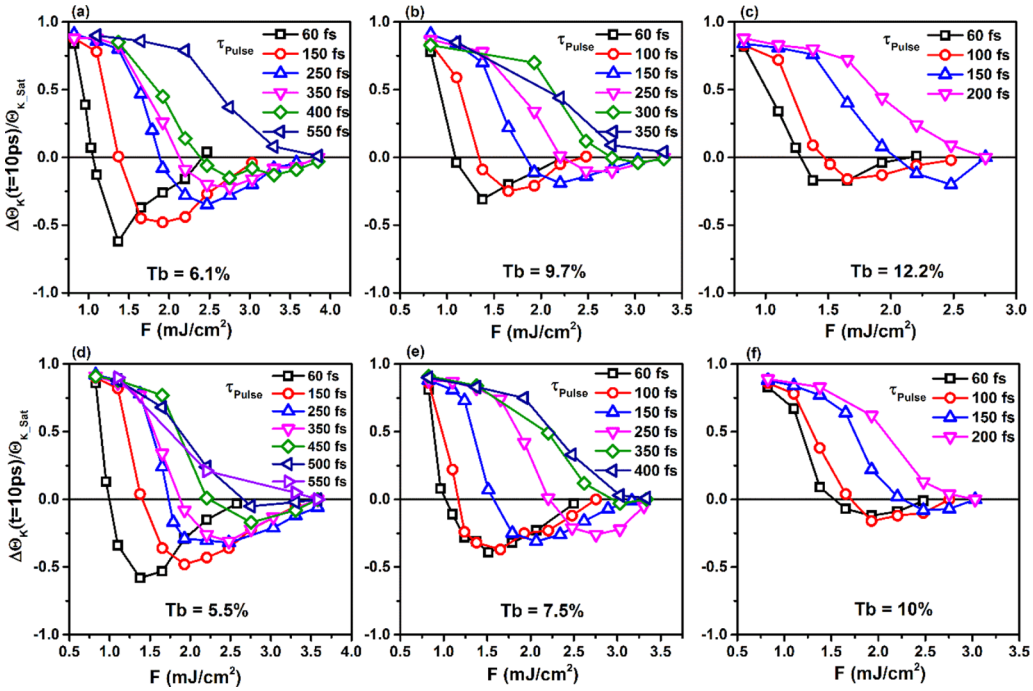

FIG. 4. Laser fluence dependence of the $\Delta\Theta_K/\Theta_{K\_sat}$ signal measured at 10 ps after excitation of samples for different laser-pulse duration and Tb concentrations. (a)–(c) correspond to $x = 78\%$ and (d)–f) correspond to the samples with $x = 80\%$.

state diagram obtained using TR-MOKE is shown in Fig. S4 to compare with the one obtained by Kerr microscopy.

To understand the effect of Tb concentration in combination with the effect of the pulse duration on AO-HIS, we measured the fluence dependence of the TR-MOKE signal at 10 ps after excitation of the samples with $x = 78\%$ shown in Figs. 4(a)–4(c) and $x = 80\%$ shown in 4(d)–4(f). Here, three different behaviors as a function of laser fluence can be clearly distinguished. Firstly, the magnetization recovers toward its initial state at low fluence for all the samples, which is evidenced by the value of $\Delta\Theta_K(10\text{ ps})/\Theta_{K\_sat} \approx 1$. Secondly, with a medium laser fluence, a long-lived partially demagnetized state is observed for all samples $[0 < \Delta\Theta_K(10\text{ ps})/\Theta_{K_{sat}} < 1]$. Finally, the AO-HIS is achieved $[\Delta\Theta_K(10\text{ ps})/\Theta_{K\_sat} < 0]$ when laser fluence raises above a threshold fluence F_{switch}. In addition to the laser fluence-dependent behavior, $\Delta\Theta_K(10\text{ ps})/\Theta_{K\_sat}$ is, more importantly, closely connected to both pulse duration as well as Tb concentration. Within the region of $\Delta\Theta_K(10\text{ ps})/\Theta_{K\_sat} < 0$, the absolute maximum value of $\Delta\Theta_K(10\text{ ps})/\Theta_{K\_sat}$ at a certain fluence decreases with the laser pulse broadening; then it becomes zero at the critical pulse duration τ_{max}. For instance, as is shown in Fig. 4(a), the value of $\Delta\Theta_K(10\text{ ps})/\Theta_{K\_sat}$ drops from -0.6 to 0 when τ_{pulse} is raised from 50 to 550 fs for the samples of $Gd_{15.9}Tb_{6.1}Co_{78}$. Meanwhile, $\Delta\Theta_K(10\text{ ps})/\Theta_{K\_sat}$ is also changed obviously by the concentration of Tb, which is evidenced by the fact that it is reduced from -0.6 to -0.2 by increasing the Tb concentration from 6.1 to 12.2% using 50-fs pulse duration [Figs 4(a) and 4(c)]. These results contrast with the fact that the demagnetization shows no dependence with the Tb concentration. This indicates the role of spin-lattice coupling effect induced by alloying Gd and Tb only works at around a few tens of picoseconds, consistent with previous TR-MOKE measurements in Gd_xTb_{1-x} alloys [27]. For the samples with $x = 80\%$, similar results are obtained as is illustrated in Figs. 4(d)–4(f).

III. ATOMISTIC MODELING FOR ULTRAFAST DEMAGNETIZATION AND SINGLE-SHOT AO-HIS

In order to understand the experimental results, atomistic simulations using the VAMPIRE software package [32] were performed on the materials $Gd_{1-x-y}Tb_yCo_x$ with $x = 80\%$, $y = 5.5$, 7.5, 9.8, and 12.5% to reproduce both ultrafast demagnetization and magnetization switching. An element-specific damping of the Gd, Tb, and Co sites was assigned separately [29], instead of using a net damping of the system, to take into account the different spin-lattice coupling between Gd and Tb. Here, we firstly fixed the element-specific damping values of 0.08 at the site of Tb to reproduce the experimental results, four times larger than 0.02 assigned to Gd and Co sites. This is reliable considering the previous theoretical and experimental studies. For instance, Rebei *et al.* [33] proposed the RE-induced damping to be proportional to the orbital moment of the dopants. And then, it was confirmed that Tb-doped NiFe film shows a strong dependence of damping on doping concentration, while Gd doping NiFe film is not influenced [34]. After reproducing our experimental results, the damping value of Tb is varied from 0.002 to 0.1 to test its influence on AO-HIS.

All optical helicity-independent switching

We simulate the laser fluence and pulse duration-dependent AO-HIS at longer timescale which agrees well with the TR-MOKE measurements, indicating the reliability of our

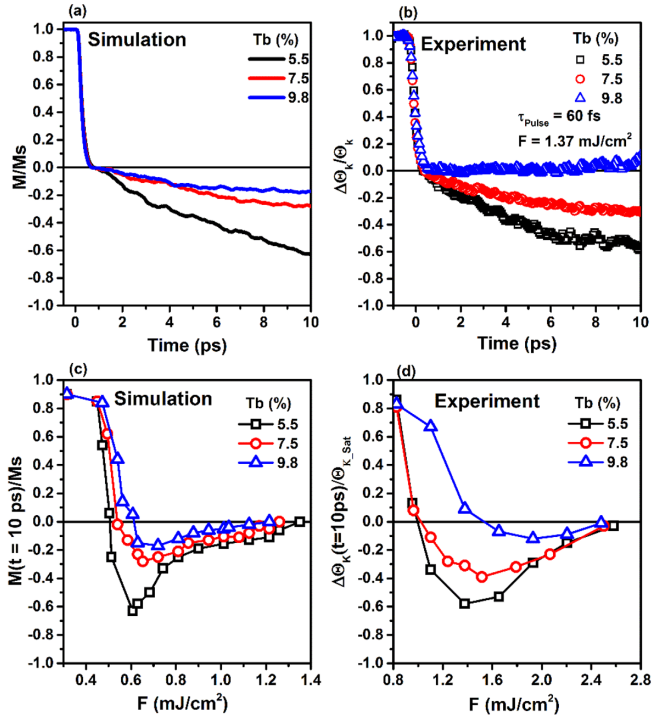

FIG. 5. Comparison of AO-HIS between simulations and experiments for the samples with $x = 80\%$. (a), (b) Magnetization dynamics of Co sublattice as a function of Tb concentration obtained by simulation and TR-MOKE measurements, respectively. (c), (d) Tb concentration-dependent normalized z component of magnetization and TR-MOKE signal obtained at 10 ps after the excitation of laser pulse.

simulations (see Fig. S6 in Note 5 of the Supplemental Material) [31]. The dynamics of the magnetization of the Co sublattice as a function of Tb concentration is shown explicitly in Fig. 5(a). For Tb = 5.5%, the magnetization rapidly drops to zero within 1 ps, and then it recovers in the opposite direction showing magnetization switching. With more Tb, all the samples share the similar initial demagnetization; however, the remagnetization process becomes slower. This trend is observed as well by TR-MOKE measurements as shown in Fig. 5(b). In the case of Tb = 9.8%, the magnetization stays around zero for several ps after the demagnetization. This state is reached when the fluence approaches F_{switch}. Further increase of the fluence leads to the reversal of magnetization. We have to address that the magnetization recovery process after switching could be changed by magnetic fields [35]. According to Note 6 of the Supplemental Material [31], however, it can be excluded here due to the different behavior induced by different applied fields starting to appear at 10 ps and becoming pronounced at 50-ps timescale. It is much longer than the timescale at which the magnetization dynamics differs by various Tb concentration, where the timescale is below 10 ps as shown in Figs. 5(a) and 5(b).

Moreover, Fig. 5(c) shows the normalized magnetization along the z component of the Co sublattice as a function of the laser fluence after 10 ps for different Tb compositions. For each sample, two values of laser fluence correspond to the zero level of magnetization. The smaller one is defined as

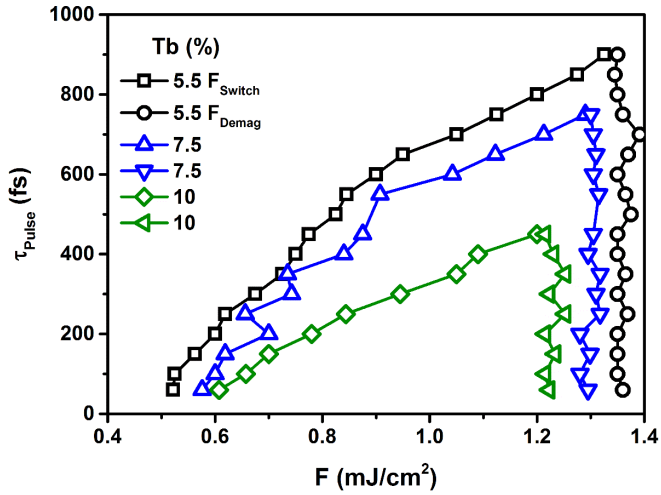

FIG. 6. AO-HIS state diagram by atomistic simulations for $x = 80\%$. Critical switching fluence F_{switch} and fully demagnetization fluence F_{demag} as a function of the pulse duration with various Tb concentration.

F_{switch}, while the larger one is F_{demag} during the simulations. As the Tb concentration increases from 5.5 to 9.8%, F_{switch} becomes larger, F_{demag} becomes slightly smaller, and the normalized magnetization is reduced from -0.6 to -0.2 in the region of $M_z(t = 10\text{ ps})/M_s < 0$. These features are in good agreement with the results obtained by TR-MOKE as shown in Fig. 5(d).

To further study the influence of the Tb concentration on the magnetization switching, we present in Fig. 6 the simulated state diagram. The laser fluence representing switching and full demagnetization is extracted from Fig. S7 of the Supplemental Material [31] for a given pulse duration. When the concentration of Tb becomes larger, F_{switch} increases and τ_{max} is reduced from 900 to 400 fs, although the evolution of F_{switch} with the pulse duration τ_{pulse} is independent of the Tb concentration. The simulated state diagrams nicely reproduce the experimental ones shown in Fig. 2 and Fig. S4. Despite this, one can see both the fluence and pulse duration allowing for single-shot switching are lower in atomistic simulations as compared with those in experiments. In the simulations, these two critical parameters are dependent on the Curie temperature T_c as well as the element-specific damping α we selected. The deviations of T_c and α used in the simulations from the experimental ones are the main reasons for the differences in F_{switch} and τ_{max}. The dependence of F_{switch} on damping is shown explicitly in the following.

IV. DISCUSSION

In this simulation, different values of Gilbert damping are assigned to Gd and Tb, respectively, to reproduce the experimental results expanding from femtosecond to picosecond timescales. In both experimental and simulated results, we found that ultrafast demagnetization time is independent of Tb composition (see Note 7, Supplemental Material) [31], while the AO-HIS phenomenon is prohibited by increasing Tb content. Our conclusions are consistent with those reported by Ceballos *et al.* [29], where the switching is vanished when

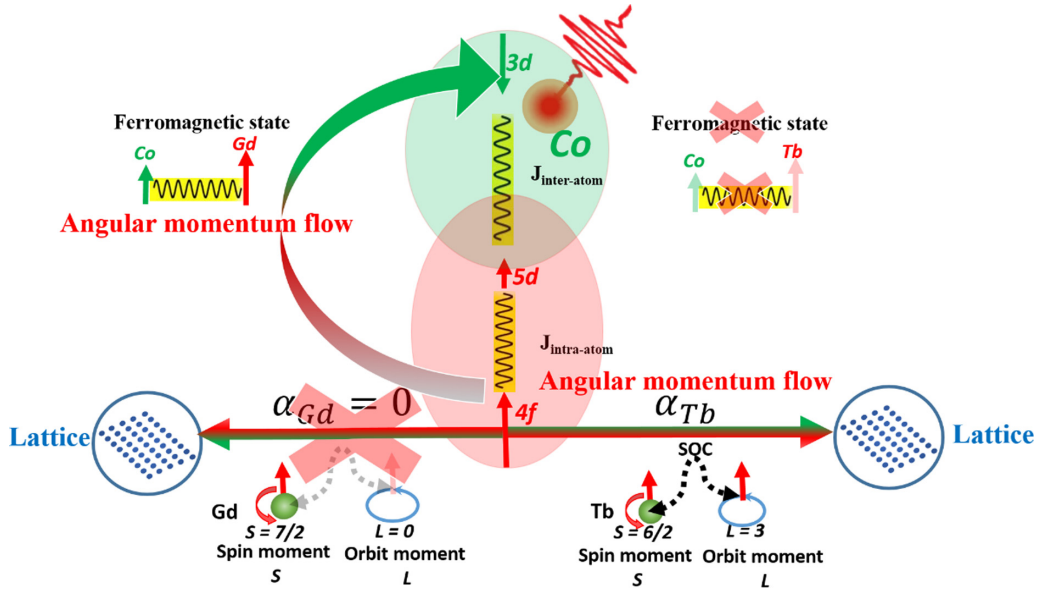

FIG. 7. Conceptual diagram for spin angular momentum dissipation process in RE-TM alloys after infrared laser excitation. The infrared laser pulse interacts with delocalized d electrons directly, leading to a strong coupling between d electrons and photon. For the localized $4f$ electrons in RE elements, they are mainly coupled to the phonon bath, but indirectly excited via $5d$-$4f$ intra-atomic exchange energy. Two processes responsible for spin angular momentum dissipation are categorized. Firstly, spin angular momentum can be dissipated by lattice, but it depends on the orbital quantum number L. For Gd, this channel is reduced a great deal due to $L = 0$ as compared to Tb, where $L = 3$. Secondly, the interaction between RE and TM facilitated by intra-atomic exchange energy provides another channel for spin angular momentum transfer.

the concentration of Tb is larger than 18% in $Gd_{22-x}Tb_xCo_{78}$. The above results can be understood based on the following phenomenological mechanism, in which we split the whole dynamic process according to the different timescales involved, as shown in Fig. 7.

(i) Ultrafast demagnetization in femtosecond timescale. In the near-infrared regime used in this experiment, the $3d$ and $5d$ delocalized electrons stemming from TM (Co) and RE (Tb and Gd) elements, respectively, can be excited directly to a nonequilibrium state [33], although the $5d$ electrons in RE metals carry only very small magnetic moments in both Gd (0.55 μ_B) and Tb (0.34 μ_B). The mechanisms underlying the ultrafast timescale dynamics are still highly debated, but it is generally accepted up to now that such ultrafast dynamics is the consequence of hot electrons induced by laser pulse. According to previous study, the time needed for ultrafast partial demagnetization of $5d$ electrons is identical for Gd and Tb single elements [36,37]. Both are around 750 fs, which is too early to see the influence of different spin-lattice coupling between Gd and Tb. Although Lopez-Flores *et al.* [38] found a faster demagnetization in Tb than in Gd within the Co-RE (RE = Gd and Tb) alloys via time-resolved x-ray magnetic circular dichroism measurements, the same demagnetization time of Co is verified in both alloys of CoTb and CoGd. In our case, the spin information comes mainly from Co sublattice due to the near-infrared laser pulse used. Thereby, replacing Gd by Tb continuously in GdTbCo is not expected to give a pronounced change of ultrafast demagnetization time τ_M of Co sublattice.

(ii) Magnetization dynamics in picoseconds. Most of the magnetism in Gd (7 μ_B) and Tb (9 μ_B) comes from the deeply buried $4f$ localized electrons, so that they cannot be excited directly by the used photon energy of 1.5 eV. Despite this, the intersublattice $3d$-$5d6s$-$4f$ exchange coupling serves as a bridge to transfer spin angular momentum between RE and TM sublattices. For Tb, this channel competes with the transfer of spin angular momentum from $4f$ electrons to the lattice due to its strong spin-orbit coupling. On the contrary, the spin-lattice coupling in Gd is blocked because of zero orbital momentum. So, the spin angular momentum is favored to transfer between Gd and Co sublattices. Therefore, alloying Gd and Tb hopefully induce a tunable spin-lattice coupling, and consequently, the magnetization dynamics as well as the magnetization switching in picoseconds are expected to depend on the concentration of Tb, as evidenced in this work.

As illustrated in Fig. 7, the spin relaxation after laser-pulse irradiation in RE elements (Gd and Tb) can occur via different channels. Firstly, the spin angular momentum is directly dissipated by the scattering between spins and lattices, depending on the value of orbital moments. Secondly, the spin angular momentum is transferred indirectly between RE (Gd Tb) and TM (Co) sublattices via interatomic exchange of $4f$-$5d6s$-$3d$ electrons [39,40]. It is worth mentioning that the above two pathways have been demonstrated recently via time-resolved photoemission spectroscopy in Gd and Tb rare-earth elements [41]. The different spin-lattice coupling in Gd and Tb leads to different magnitude of the spin-relaxation rates, and consequently different spin dynamics as well as AO-HIS behaviors when Gd and Tb concentrations are varied.

Considering the good agreement between experiments and simulations, we propose that the difference in magnetization dynamics taking place at a few picosecond timescale with various Tb concentration is attributed to the larger spin-lattice coupling in Tb as compared with Gd. To explore the effect of

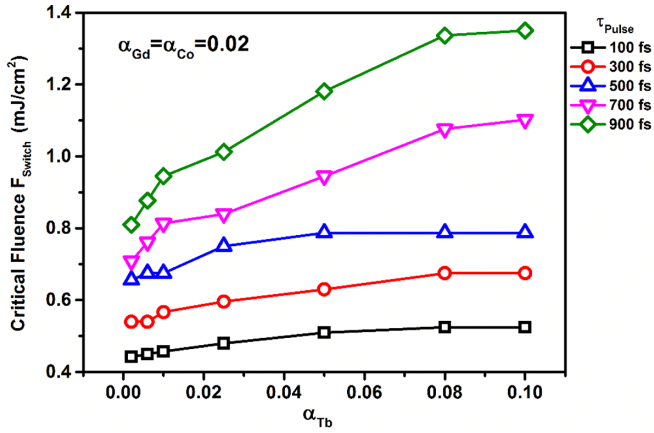

FIG. 8. The evolution of F_{switch} as a function of Gilbert damping parameter of Tb with different laser-pulse duration τ_{pulse}.

Gilbert damping further, it was tuned in the range of 0.002 to 0.1 to study the sensitivity of F_{switch} to the elementary spin-lattice coupling effect as is shown in Fig. 8. Meanwhile, the laser-pulse duration is another external parameter to tune spin dynamics as is shown in the experiments. One can see the minimum F_{switch} is observed at the shortest laser-pulse duration, which is independent of the damping parameter. At a given laser-pulse duration, F_{switch} increases monotonously with larger damping of Tb. From a phenomenological viewpoint, a larger damping of RE results in a stronger spin-lattice coupling, suggesting more spin angular momentum is dissipated via the scattering of spins and phonons. Therefore, less spin angular momentum is flowed between RE and TM elements, which is, however, the main driving force to switch the magnetization in RE-TM alloys. In this case, a much larger laser fluence is needed to compensate the spin angular momentum dissipated by the lattice in order to present AO-HIS.

Based on our experiments and simulations, the magnetization switching is vanished in GdTbCo alloy by increasing Tb content due to the too large damping for Tb. In this case, the transfer of spin angular momentum between RE (Gd Tb) and TM (Co) is reduced when the concentration of Tb increases and leads to a slower remagnetization of Co in the timescale of a few picoseconds. Both the calculated and experimental results as well as the model proposed in Fig. 8 can partially explain why Gd-based RE-TM is relatively easier to show AO-HIS compared with Tb-based RE-TM structures. Apart from the prerequisite of substantial different spin dynamics for RE and TM sublattices, the sample compensation T_{comp} [42] or Curie temperature T_c [19] also play a key role in determining the parameters for the occurrence of AO-HIS such as τ_{max}, $F_{switch,}$ and F_{demag}. In particular, the demagnetization speed of RE could be tuned by engineering Co-RE samples with different T_{comp} and T_c. For instance, a faster demagnetization of Tb was observed in $Co_{74}Tb_{26}$ than $Co_{86}Tb_{14}$ because the excited-state temperature was in the vicinity of T_{comp} and T_c for $Co_{74}Tb_{26}$ and $Co_{86}Tb_{14}$, respectively [38]. However, in this study, we mainly focus on the different spin dynamics induced by varied Gilbert damping in a series of GdTbCo samples. To understand the combined effect from both magnetization dynamics and compensation or Curie temperatures, many more samples expending from RE dominant to TM dominant should be deposited, which goes beyond the scope of this study.

V. CONCLUSION

By engineering a series of $Gd_{1-x-y}Tb_yCo_x$ samples, we studied the influence of the spin-lattice coupling in the magnetization dynamic leading to all optical helicity-independent switching. Indeed, Gd shows little spin-orbit coupling allowing angular momentum transfer from Gd to Co, whereas Tb shows strong spin-orbit coupling which facilitates the angular momentum transfer to the lattice. We demonstrated that low Tb composition allows the observation of AO-HIS on a larger range of laser fluence. Furthermore, it is found that the ultrafast demagnetization of GdTbCo alloy taking place at femtosecond timescale is independent of Tb concentration, while the TR-MOKE signal measured at 10 ps after laser-pulse excitation becomes smaller with more Tb when AO-HIS occurs. In order to understand the role of spin-lattice coupling on ultrafast and fast timescales, we simulate the ultrafast demagnetization process as well as AO-HIS in GdTbCo alloys via assigning an element-specific damping between Gd and Tb. A good agreement is found between experiment and simulation.

ACKNOWLEDGMENTS

This work has been supported by the European Union's Horizon 2020 research and innovation programme COMRAD under the Marie Skłodowska-Curie Grant Agreement No. 861300, by FEDER-FSE Lorraine et Massif des Vosges 2014–2020, a European Union Program, by Institut Carnot ICEEL, Region Grand Est, by the impact Project No. LUE-N4S part of the French PIA project "Lorraine Université d'Excellence," Reference No. ANR-15IDEX-04-LUE and the ANR UFO (Grant No. ANR-20-CE09-0013). It is based upon work from COST Action Grant No. CA17123 MAGNETOFON, supported by COST (European Cooperation in Science and Technology). The authors gratefully acknowledge the National Natural Science Foundation of China (Grants No. 11904016, No. 12104030, and No. 61627813), and Beihang Hefei Innovation Research Institute Project (Grants No. BHKX-19-01 and No. BHKX-19-02).

[1] A. V. Kimel and M. Li, Nat. Rev. Mater. **4**, 189 (2019).
[2] Y. S. Liu, H. Y. Cheng, Y. Xu, P. Vallobra, S. Eimer, X. Q. Zhang, X. J. Wu, T. X. Nie, and W. S. Zhao, Phys. Rev. B **104**, 064419 (2021).
[3] X. Xiang, T. Zhu, F. Sheng, Z. Zhang, and J. Xiao, IEEE Trans. Magn. **39**, 2770 (2003).
[4] R. O. Cherifi, V. Ivanovskaya, L. C. Phillips, A. Zobelli, I. C. Infante, E. Jacquet, V. Garcia, S. Fusil, P. R. Briddon, N. Guiblin, A. Mougin, A. A. Ünal, F. Kronast, S. Valencia, B. Dkhil, A. Barthélémy, and M. Bibes, Nat. Mater. **13**, 345 (2014).
[5] Z. Li and S. Zhang, Phys. Rev. B **69**, 134416 (2004).

[6] O. Kovalenko, T. Pezeril, and V. V. Temnov, Phys. Rev. Lett. **110**, 266602 (2013).

[7] D. C. Ralph and M. D. Stiles, J. Magn. Magn. Mater. **320**, 1190 (2008).

[8] Y. Cao, Y. Sheng, K. W. Edmonds, Y. Ji, H. Z. Zheng, and K. Y. Wang, Adv. Mater. **32**, 1907929 (2020).

[9] C. D. Stanciu, F. Hansteen, A. V. Kimel, A. Kirilyuk, A. Tsukamoto, A. Itoh, and T. Rasing, Phys. Rev. Lett. **99**, 047601 (2007).

[10] I. Radu, K. Vahaplar, C. Stamm, T. Kachel, N. Pontius, H. A. Dürr, T. A. Ostler, J. Barker, R. F. L. Evans, R. W. Chantrell, A. Tsukamoto, A. Itoh, A. Kirilyuk, T. Rasing, and A. V. Kimel, Nature (London) **472**, 205 (2011).

[11] J. Walowski and M. Munzenberg, J. Appl. Phys. **120**, 140901 (2016).

[12] C. S. Davies, T. Janssen, J. H. Mentink, A. Tsukamoto, A. V. Kimel, A. F. G. van der Meer, A. Stupakiewicz, and A. Kirilyuk, Phys. Rev. Appl. **13**, 024064 (2020).

[13] Y. Xu, M. Hehn, W. Zhao, X. Lin, G. Malinowski, and S. Mangin, Phys. Rev. B **100**, 064424 (2019).

[14] A. El-Ghazaly, B. Tran, A. Ceballos, C.-H. Lambert, A. Pattabi, S. Salahudin, F. Hellman, and J. Bokor, Appl. Phys. Lett. **114**, 232407 (2019).

[15] M. L. M. Lalieu, M. J. G. Peeters, S. R. R. Haenen, R. Lavrijsen, and B. Koopmans, Phys. Rev. B **96**, 220411 (2017).

[16] J. Gorchon, C.-H. Lambert, Y. Yang, A. Pattabi, R. B. Wilson, S. Salahud- din, and J. Bokor, Appl. Phys. Lett. **111**, 042401 (2017).

[17] F. Jakobs, T. A. Ostler, C.-H. Lambert, Y. Yang, S. Salahuddin, R. B. Wilson, J. Gorchon, J. Bokor, and U. Atxitia, Phys. Rev. B **103**, 104422 (2021).

[18] J. Gorchon, R. B. Wilson, Y. Yang, A. Pattabi, J. Y. Chen, L. He, J. P. Wang, M. Li, and J. Bokor, Phys. Rev. B **94**, 184406 (2016).

[19] J. Q. Wei, B. Y. Zhang, M. Hehn, W. Zhang, G. Malinowski, Y. Xu, W. S. Zhao, and S. Mangin, Phys. Rev. Appl. **15**, 054065 (2021).

[20] M. Dąbrowski, J. N. Scott, W. R. Hendren, C. M. Forbes, A. Frisk, D. M. Burn, D. G. Newman, C. R. J. Sait, P. S. Keatley, A. T. N'Diaye, T. Hesjedal, G. van der Laan, R. M. Bowman, and R. J. Hicken, Nano Lett. **21**, 9210 (2021).

[21] C. Banerjee, N. Teichert, K. E. Siewierska, Z. Gercsi, G. Y. P. Atcheson, P. Stamenov, K. Rode, J. M. D. Coey, and J. Besbas, Nat. Commun. **11**, 4444 (2020).

[22] L. Avilés-Félix, A. Olivier, G. Li, C. S. Davies, L. Álvaro-Gómez, M. Rubio-Roy, S. Auffret, A. Kirilyuk, A. V. Kimel, Th. Rasing, L. D. Buda-Prejbeanu, R. C. Sousa, B. Dieny, and I. L. Prejbeanu, Sci. Rep. **10**, 5211 (2020).

[23] S. Alebrand, U. Bierbrauer, M. Hehn, M. Gottwald, O. Schmitt, D. Steil, E. E. Fullerton, S. Mangin, M. Cinchetti, and M. Aeschlimann, Phys. Rev. B **89**, 144404 (2014).

[24] T. M. Liu, T. H. Wang, A. H. Reid, M. Savoini, X. F. Wu, B. Koene, P. Granitzka, C. E. Graves, D. J. Higley, Z. Chen, G. Razinskas, M. Hantschmann, A. Scherz, J. Stöhr, A. Tsukamoto, B. Hecht, A. V. Kimel, A. Kirilyuk, T. Rasing, and H. A. Dürr, Nano Lett. **15**, 6862 (2015).

[25] L. Avilés-Félix, L. Álvaro-Gómez, G. Li, C. S. Davies, A. Olivier, M. Rubio-Roy, S. Auffret, A. Kirilyuk, A. V. Kime, Th. Rasing, L. D. Buda-Prejbeanu, R. C. Sousa, B. Dieny, and I. L. Prejbeanu, AIP Adv. **9**, 125328 (2019).

[26] R. Moreno, T. A. Ostler, R. W. Chantrell, and O. Chubykalo-Fesenko, Phys. Rev. B **96**, 014409 (2017).

[27] A. Eschenlohr, M. Sultan, A. Melnikov, N. Bergeard, J. Wieczorek, T. Kachel, C. Stamm, and U. Bovensiepen, Phys. Rev. B **89**, 214423 (2014).

[28] B. Andres, S. E. Lee, and M. Weinelt, Appl. Phys. Lett. **119**, 182404 (2021).

[29] A. Ceballos, A. Pattabi, A. El-Ghazaly, S. Ruta, C. P. Simon, R. F. L. Evans, T. Ostler, R. W. Chantrell, E. Kennedy, M. Scott, J. Bokor, and F. Hellman, Phys. Rev. B **103**, 024438 (2021).

[30] R. F. L. Evans,W. J. Fan, P. Chureemart, T. A. Ostler, M. O. A. Ellis, and R. W. Chantrell, J. Phys.: Condens. Matter **26**, 103202 (2014).

[31] See Supplemental Material at http://link.aps.org/supplemental/10.1103/PhysRevB.105.054410 for static loop measurements obtained by MOKE technique, static diagram, ultrafast demagnetization dynamics, field-dependent all optical switching obtained by TR-MOKE dynamics, and the details for atomistic spin modeling.

[32] VAMPIRE software package. Available from https://vampire.york.ac.uk/.

[33] A. Rebei and J. Hohlfeld, Phys. Rev. Lett. **97**, 117601 (2006).

[34] G. Woltersdorf, M. Kiessling, G. Meyer, J.-U. Thiele, and C.-H. Back, Phys. Rev. Lett. **102**, 257602 (2009).

[35] M. J. G. Peeters, Y. M. van Ballegooie, and B. Koopmans, Phys. Rev. B **105**, 014429 (2022).

[36] B. Koopmans, G. Malinowski, F. Dalla Longa, D. Steiauf, M. Fähnle, T. Roth, M. Cinchetti, and M. Aeschlimann, Nat. Mater. **9**, 259 (2010).

[37] A. Melnikov, I. Razdolski, T. O. Wehling, E. T. Papaioannou, V. Roddatis, P. Fumagalli, O. Aktsipetrov, A. I. Lichtenstein, and U. Bovensiepen, Phys. Rev. Lett. **107**, 076601 (2011).

[38] V. López-Flores, N. Bergeard, V. Halté, C. Stamm, N. Pontius, M. Hehn, E. Otero, E. Beaurepaire, and C. Boeglin, Phys. Rev. B **87**, 214412 (2013).

[39] A. Mekonnen, A. R. Khorsand, M. Cormier, A. V. Kimel, A. Kirilyuk, A. Hrabec, L. Ranno, A. Tsukamoto, A. Itoh, and Th. Rasing, Phys. Rev. B **87**, 180406(R) (2013).

[40] B. Frietsch, J. Bowlan, R. Carley, M. Teichmann, S. Wienholdt, D. Hinzke, U. Nowak, K. Carva, P. M. Oppeneer, and M. Weinelt, Nat. Commun. **6**, 8262 (2015).

[41] B. Frietsch, A. Donges, R. Carley, M. Teichmann, J. Bowlan, K. Döbrich, K. Carva, D. Legut, P. M. Oppeneer, U. Nowak, and M. Weinelt, Sci. Adv. **6**, eabb1601 (2020).

[42] V. N. Gridnev, Phys. Rev. B **100**, 174405 (2019).